# Risk-Aware Routing for Uncrewed Aircraft Contingency Management

Vishwanath Bulusu*, Nadezhda Dimitrova†, Jordan Sakakeeny‡, William Ward§, and Husni Idris¶
*NASA Ames Research Center, Moffett Field, CA, USA*

**This paper investigates the impact of risk-aware routing of uncrewed aircraft on airspace operations during a contingency. Loss of command and control link is the contingency modeled. Amidst such a contingency, uncrewed aircraft are routed based on interaction risk derived from the last known traffic predictions in the airspace en route to a destination. These risk-aware routes are compared with the last cleared nominal routes (without information on traffic prediction) using fast-time simulations. Impacts on safety and operational efficiency are measured. Impacts are measured for a fleet of uncrewed aircraft, and compared between entries into the terminal airspace from four different directions. Routing based on interaction risk from visual and instrument flight rules traffic is considered. Results showed an improvement in safety and efficiency when accounting for traffic interaction risk.**

## I. Introduction

The introduction of Uncrewed Aircraft (UA) for regional cargo operations necessitates safe integration with legacy crewed traffic. Likely initial operations will employ remotely piloted large fixed-wing Uncrewed Aircraft Systems (UAS) [1]. A typical operation is expected to involve a Remote Pilot (RP) operating the UA from a Ground Station (GS) under Instrument Flight Rules (IFR). It will entail interaction with Air Traffic Control (ATC) services and other crewed traffic. The lack of an onboard pilot makes handling in-flight contingencies a crucial barrier to safe integration in the airspace [2]. This paper investigates the impact of traffic interaction risk-aware routing of UA on safe operations amidst a contingency in terminal airspace.

The RP operates the UA via a command and control (C2) link system [3], hereafter shortened to "C2 link". The loss of the C2 link (LC2L) is an important contingency to evaluate, and the ability to handle it is a key barrier to entry. Hence, LC2L is the contingency modeled in this paper. An LC2L can have multiple levels of severity such as loss of radio, uplink, and/or downlink. However, for simplicity and to evaluate the “worst-case scenario”, the LC2L event in this work will refer to the total severance of the C2 link system where the link will not be re-established. In an LC2L state, the RP cannot upload data to, or receive data from the UA, nor are they able to relay voice communications via the UA.

To ensure predictability during an LC2L event, prior research has proposed LC2L procedures for UA. For example, a 2020 International Civil Aviation Organization (ICAO) working paper built LC2L procedures from existing radio communication failure (commonly called "NORDO") procedures [4]. It distinguished procedure requirements between terminal and en route airspace. Developing further on this ICAO work and current Federal Aviation Agency (FAA) UAS policy and regulations, in 2023, the RTCA, Inc. Special Committee 228 (SC-228) published “Guidance Material: Standardized Lost C2 Link Procedures for Uncrewed Aircraft Systems”, also referred to as “DO-400” [5]. It splits actions across eight phases of flight: preflight, taxi, takeoff, climb out/departure, transit/extended UA operations, arrival/approach, landing, and post-flight. It also prescribes actions for the RP and ATC during an LC2L event and identifies differences for non-towered airports. Prior work conducted an initial assessment of these LC2L procedures in a simulated representative terminal airspace environment [6]. The previous works identified the need to account for factors such as surrounding traffic density and airspace complexity to improve the safety and efficiency of UA operations in contingency situations.

This study, therefore, explores the impact of altering the LC2L procedures, accounting for surrounding traffic. The work focuses on the terminal phases of UA flight. Legacy traffic (e.g., conventionally crewed traffic such as airliners and general aviation) in the terminal environment operates under IFR and Visual Flight Rules (VFR), with the latter

*Aerospace Research Scientist, Crown Consulting Inc., Aviation Systems Division, AIAA Member
†Simulations Engineer, Metis Technology Solutions Inc., Aviation Systems Division, AIAA Member
‡Aerospace Engineer, Aviation Systems Division, AIAA Member
§Research Engineer, Oden Institute for Computational Engineering and Sciences, University of Texas at Austin
¶Aerospace Research Engineer, Aviation Systems Division, AIAA Associate Fellow

being a major proportion of the traffic [7]. To support UA operations amidst legacy traffic, models were developed to predict VFR and IFR traffic behavior in a terminal environment [7–9]. Interaction risk with traffic was captured as predictive occupancy maps showing the spatio-temporal probability of interaction with legacy traffic. The current work uses legacy traffic prediction to create UA routes that minimize traffic interaction risk during an LC2L event. The safety and efficiency impacts of using such routes are compared with operation under nominal and DO-400 procedures.

The rest of the paper is structured as follows. Section II discusses the overall experiment design, metric-informed trajectory planning, test scenarios, scenario evaluation metrics, and study assumptions. Results are presented in Section III. The authors note that other factors could be accounted for during trajectory planning beyond simply traffic interaction risk. In an accompanying extension of this work [10], the authors evaluate tradeoffs between minimizing communication task load and traffic interaction risk during contingency management.

## II. Methodology

This section describes the experiment design, metric-informed trajectory planning, test scenarios for evaluation, scenario evaluation metrics, and the study assumptions.

### A. Experiment Design

NASA's National Airspace System (NAS) Digital Twin simulation environment [11] is used to model the traffic and terminal airspace operational procedures and evaluate risk-aware routing. Built off of the NASA ATM TestBed software platform [12, 13], NAS Digital Twin is composed of a modular architecture to verify and validate new concepts and technologies, simulate changes to the NAS, and uncover unintended consequences and risks of introducing new concepts and technologies.

During a nominal arrival procedure, the UA is assumed to operate under IFR and continue on a Standard Terminal Arrival Procedure (STAR) that funnels it from the Air Route Traffic Control Center (ARTCC) or "Center" into the Terminal Radar Approach Control (TRACON) or "terminal" area. From there it is vectored by the ATC to an Instrument Approach Procedure (IAP). Both these steps are simulated as a "nominal route" in NAS Digital Twin. The DO-400 document guidelines prescribe that after reaching its last clearance before the LC2L event, the UA should proceed to the Initial Approach Fix (IAF), if not established on a STAR, or complete the STAR and then proceed to the IAF if established on a STAR. After reaching the IAF, the UA should execute the published approach through the Intermediate Fix (IF) and the Final Approach Fix (FAF) to the runway. NAS Digital Twin employs waypoint-to-waypoint (with altitude and speed constraints) trajectories to simulate the LC2L procedure.

In this work, additional route alternatives are generated based on interaction risk with VFR and IFR traffic. It is assumed that, instead of the nominal route and the published LC2L procedure, after entering the TRACON area, the UA flies straight to the IF for the final approach to the runway using routes that minimize the risk of interaction with predicted traffic. The waypoint navigation capability of NAS Digital Twin is used to simulate this. Five different route alternatives are then compared: nominal, DO-400 LC2L procedure, VFR aware route, IFR aware route, and combined VFR-IFR aware route. Legacy traffic is simulated in the background by NAS Digital Twin for a chosen test day. The impacts of different route alternatives on UA interaction with legacy traffic are thereby evaluated.

The traffic interaction risk-based trajectory planning procedure is described next. The study region and the detailed test scenarios are described under the Test Scenarios section. followed by the evaluation criteria used for the study to compare the trajectories.

### B. Metric-Informed Trajectory Planning

Traffic interaction Risk is computed spatially across an airspace region to generate cost matrices suitable for trajectory planning algorithms. Following the approach in prior work [7, 8], the analysis domain is discretized into a grid centered on the study region (terminal airspace around Fort Worth Alliance Airport (KAFW) in this work). For each cell $i$ in this grid, the corresponding cost values used in path planning are assigned directly from the computed metric probabilities derived from the historical data analysis:

$$C_{\text{interaction\_risk}}(i) = X_i = P(A \geq 1 \text{ in cell } i)$$

The spatial distribution of this cost is visualized in Figure 1 spanning a $100 \times 100$ nmi region of terminal airspace centered on KAFW under 4000 feet MSL. Brighter regions indicate a higher interaction risk. High-risk IFR corridors are visible near major airports (Dallas-Fort Worth International Airport (KDFW) and Dallas Love Field (KDAL)), reflecting structured arrival and departure flows. VFR interaction risk is more dispersed, highlighting the spatial and

temporal variability introduced by flexible routing near satellite airports, and is largely absent in the Class B surrounding KDFW and KDAL.

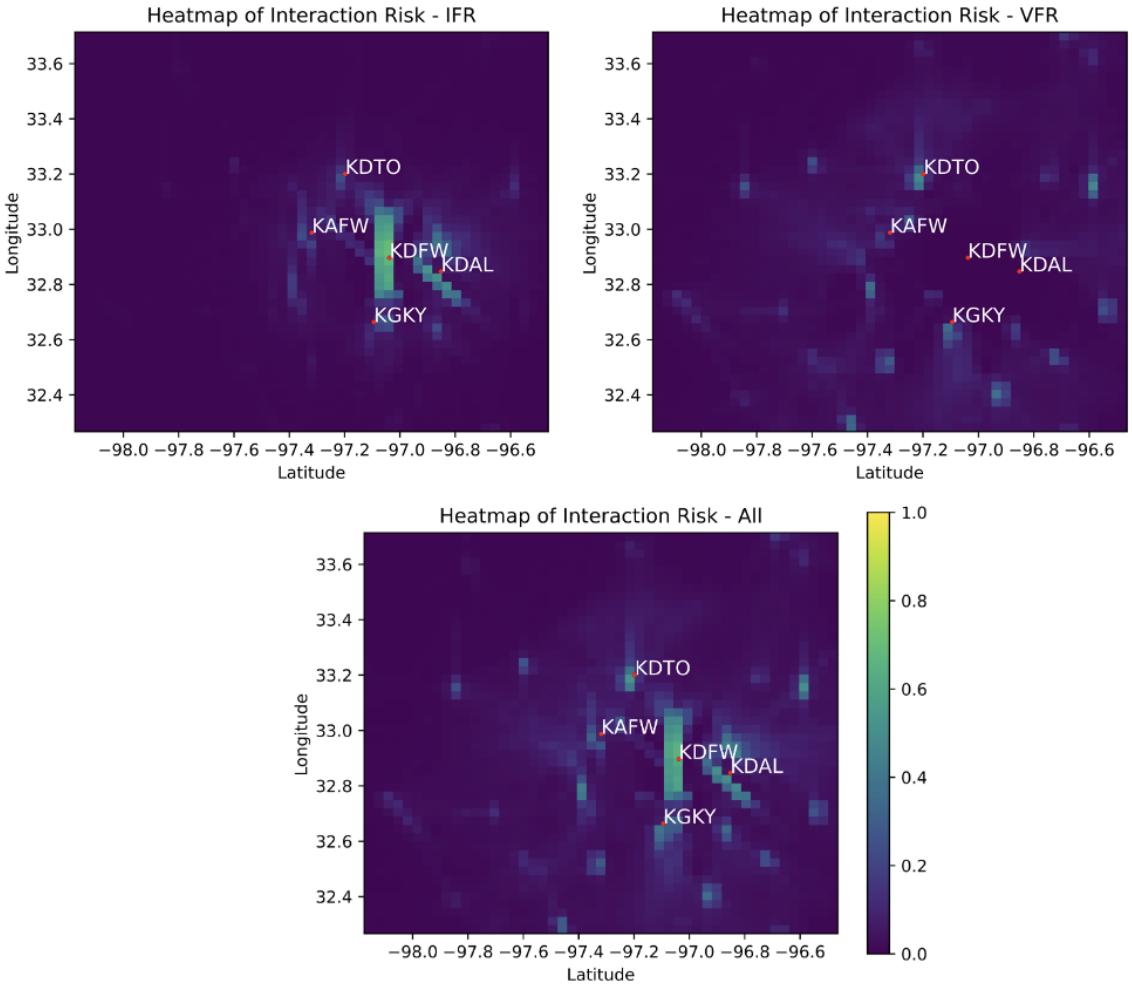


**Fig. 1 Spatial distribution of traffic interaction risk under 4000 feet MSL in the Dallas-Fort Worth terminal airspace.**

These cost matrices serve as the foundational inputs for the normalization, weighting, and path-finding processes integral to the metric-informed trajectory planning approach. Strategic trajectory planning in complex airspace necessitates balancing multiple objectives, such as minimizing flight distance and avoiding regions of high interaction risk. The outlined approach employs Dijkstra's algorithm and Pareto optimization to identify optimal paths based on normalized and weighted airspace cost-metrics matrices.

Dijkstra's shortest path algorithm is used to minimize the distance and the cumulative costs across an airspace region. The airspace is represented as a grid, where each cell $i$ is assigned a cost as described above. Additionally, a baseline $C_{\text{distance}}$ metric, representing the distance to traverse a cell, is also taken into consideration. This metric has a uniform cost of 1 per cell.

To systematically explore the trade-offs between competing objectives - specifically, $C_{\text{interaction\_risk}}$ and $C_{\text{distance}}$, Pareto optimization is employed. The Pareto Frontier comprises a set of non-dominated solutions: trajectories where improving one objective (e.g., reducing metric cost) necessarily degrades another (e.g., increases travel distance). It is constructed by repeatedly solving the path-planning problem using Dijkstra's algorithm. Each of the minimized-cost paths represents an optimal solution for a specific trade-off preference. The collection of these paths forms the Pareto

Frontier (an example is given in Figure 2), allowing for an analysis of the spectrum of achievable trade-offs and aiding in the selection of paths that best align with overarching mission requirements and resource constraints [14].

The figure illustrates the Pareto Frontier's utility for balancing costs. The top panels display example trajectories (Path 1 and Path 2) on a traffic interaction risk map, while the bottom plot shows the corresponding Pareto Frontier. Each point on this frontier is a non-dominated solution, meaning improving one objective (e.g., lower VFR interaction risk in Path 1, lower distance travelled in Path 2) necessitates a trade-off in the other (e.g., increased distance in Path 1, higher VFR interaction risk in Path 2). This frontier thus presents a spectrum of optimal trade-offs, enabling informed trajectory selection based on mission priorities between safety and efficiency.

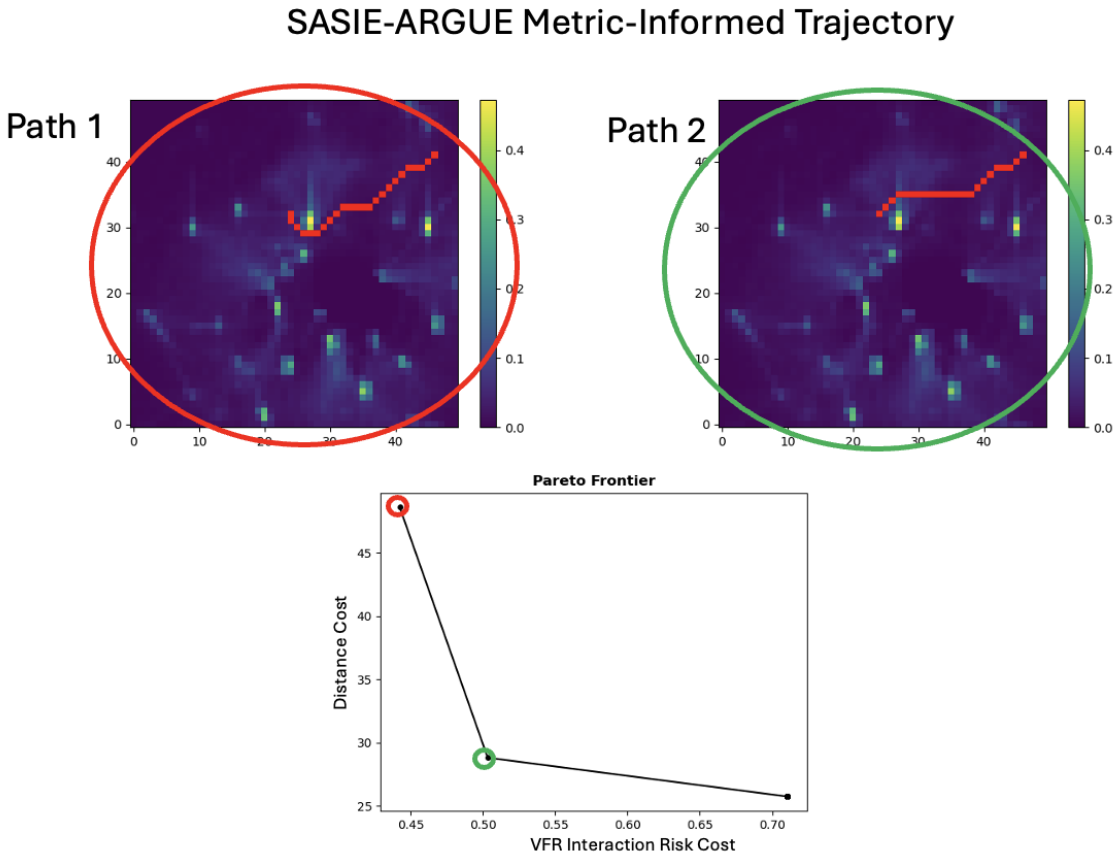


**Fig. 2 Pareto Frontier for a multi-objective trajectory planning for KAFW arrival route from a north-east entry.**

To convert multi-objective optimization into a single-objective optimization, disparate metric units are normalized to be meaningfully combined into a single cost function. This requires the construction of a normalization that respects the geometry of the Pareto Frontier.

Let $\mathcal{P} \subset \mathbb{R}^d$ denote the set of Pareto-optimal paths, and let $\{C^k\}_{k=1}^K$ be the empirical objective vectors sampled from $\mathcal{P}$. The scalarization weights $\lambda_i$ are subsequently computed as density ratios. Formally, $\lambda_i$ approximates a Radon-Nikodym (RN) derivative, which quantifies how one "density" changes relative to another across the Pareto front [15], e.g., summing over all Pareto-optimal paths. While RN derivatives generalize this idea to infinite-dimensional spaces, our finite sum ratio is its empirical counterpart:

$$\lambda_{\text{metric\_i}} = \frac{\sum_{k=1}^{K} C^k_{\text{distance}}}{\sum_{k=1}^{K} C^k_{\text{metric\_i}}}$$

Using $\lambda_i$ to normalize units constructs a quasi-convex scalarization where the weights $\lambda_i$ are nonparametric estimators of the inverse marginal rates of substitution (MRS) between objectives [16]. As more Pareto-optimal paths are sampled ($K \to \infty$), $\lambda_i$ converges to the hypervolume-maximizing scalarization - a theoretical guarantee from multi-objective optimization that ensures weights align with the Pareto front's geometry[17–19]. This avoids subjective normalization and ensures solutions are operationally relevant. The normalized cost matrices are then calculated as:

$$C_{\text{metric\_i\_normed}} = \lambda_{\text{metric\_i}} C_{\text{metric\_i}}$$

The resultant normalized cost matrices embed the Pareto front's geometry into a Lipschitz-continuous scalarized objective, thereby enabling gradient-based optimization with provable convergence to $\mathcal{P}$-aligned solutions [20, 21]. These normalized matrices, along with $C_{\text{distance}}$, form the basis for constructing final weighted cost-metric matrices for each cell:

$$C_{\text{total}} = w_{\text{metric\_i}} C_{\text{metric\_i\_normed}} \;\; w_{\text{distance}} C_{\text{distance}}$$

The weights reflect the priority assigned to minimizing each respective cost component. The process of weight tuning is crucial for investigating various mission objectives and trade-offs. Weights can be manually set to reflect specific mission priorities (e.g., safety-critical vs. efficiency-driven) or systematically varied. For instance, if minimizing traffic interaction risk is deemed twice as important as minimizing distance, $w_{\text{interaction\_risk}}$ could be set to $2 \times w_{\text{distance}}$. Future work will involve sensitivity analysis to understand the impact of each metric's weight, exploration of adaptive weight adjustments, and incorporation of subject matter expert (SME) stakeholder input to assess route acceptability and refine weight configurations.

For the primary trajectory generation and analysis presented in this study, a baseline uniform weighting scheme is adopted for the total cost function ($C_{\text{total}}$) used by the Dijkstra algorithm. Unit weights are applied to each component to establish a reference case where avoidance of traffic interactions and minimizing travel distance are considered equally important. Therefore, for this analysis, we set $w_{\text{risk}} = 1$, and $w_{\text{dist}} = 1$. In an accompanying work by the authors, this trajectory planning approach is extended to another metric measuring communication task load. Trajectories generated using this equal-priority weighting serve as the basis for evaluations.

Finally, by integrating Dijkstra's algorithm with Pareto optimization, this approach enables autonomous aircraft to plan trajectories that align with multiple mission objectives. The Pareto Frontier provides a spectrum of viable paths, allowing stakeholders to make informed decisions based on specific operational priorities. Fig. 5 from Section III shows a sample final trajectory generated by this method and discussed further in the results.

### C. Test Scenarios

KAFW was chosen as a representative cargo airport to simulate and measure impacts. KAFW is located in the northwest of the Dallas-Fort Worth metroplex and is a busy cargo hub, serving as a focus airport for both FedEx and Amazon Air. Previous research has identified KAFW as a prime candidate for initial regional air cargo operations using UAS [22]. As seen in Fig. 3, KAFW is a Class D airspace environment, located underneath the Class B airspace shelf of KDFW and KDAL. Several other Class D environments are located nearby KAFW, including two general aviation airports (Fort Worth Meacham (KFTW), Denton Enterprise (KDTO)) and a military airbase (Naval Air Station Joint Reserve Base Fort Worth (KNFW)). KAFW also hosts a continuously operating control tower and two 11,000 ft runways. One of these runways, 16L/34R, hosts an Instrument Landing System (ILS) approach on both ends, including a Category (CAT) II-III ILS approach on runway 16L.

The Dallas-Fort Worth TRACON area ("D10") surrounds the busy metroplex environment. The TRACON is a large square with its corners cut off, shown in light gray in Fig. 4. Generally, IFR flights will depart the TRACON along the flat edges of the square (to the north, east, south, or west). Arriving flights will be ushered through the four "corner posts" of D10 (i.e., northeast, southeast, southwest, and northwest). Aircraft arriving at KAFW will typically utilize one of seven STARs. These will typically end at the TRACON boundary, where the aircraft gets handed over to the TRACON controller. In this work, the LC2L route alternatives are generated from these entry points.

To evaluate entry into each of the four D10 corner posts, routes from four different origin airports were chosen - Lubbock (KLBB for northwest entry), Austin (KAUS for southwest entry), Shreveport (KSHV for southeast entry), and Little Rock (KLIT for northeast entry). Fig. 4 shows the nominal routes for each of these entries.

A total of five scenarios are evaluated and compared for each entry. Each scenario corresponds to one of the five route alternatives - Nominal, LC2L, VFR Risk-Aware, IFR Risk-Aware, and VFR+IFR Risk-Aware. The Nominal scenario is a baseline where the aircraft flies as though no contingency as occurred (akin to ATC vectoring after finishing the STAR). The LC2L scenario is also a secondary baseline where the aircraft adheres to the DO-400 guidance (proceed

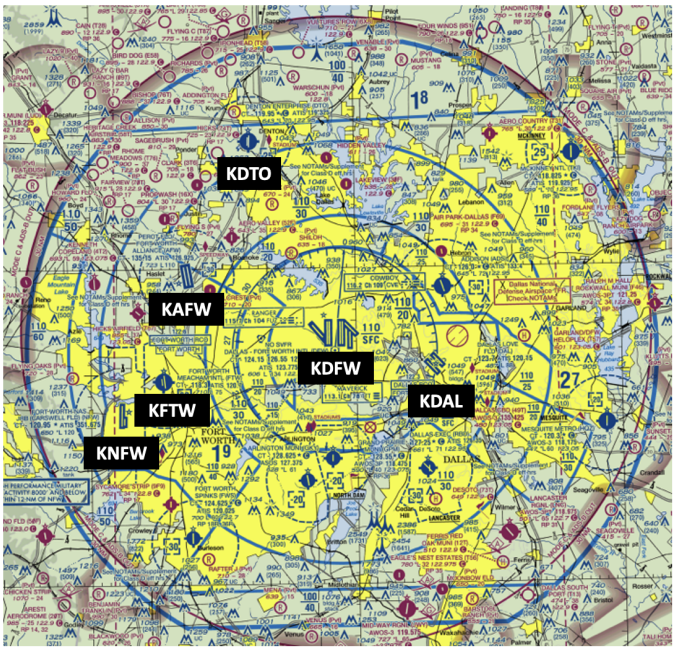


**Fig. 3 The Dallas-Fort-Worth Terminal Area on a VFR sectional chart [23] showing controlled airspace.**

to IAF, if not established on a STAR, or complete the STAR, then proceed to IAF otherwise). The remaining three scenarios account for interaction risk with VFR traffic, IFR traffic, or both. In each of these three, the route from corner entry post to the IF is determined based on the respective traffic interaction risk map as described under flight planning above. The detailed routes (with the waypoints) for the different scenarios are listed under the Appendix A. LC2L and VFR-Aware routes for southwest entry from KAUS are also depicted in Fig. 4.

For background traffic, a sample date of October 10, 2022, was used, as it represented a nominal weekday with minimal convective weather in the Fort Worth Center as indicated by the Weather-Impacted Traffic Index and delay statistics for the day. In each simulation, around 4,575 recorded flights (both IFR and VFR) from Fort Worth Center, adjacent Centers (Albuquerque, Kansas City, Memphis, and Houston), and their respective major TRACONs (D10, ABQ, MCI, T75, and I90) on that day from around 1400 to 1800 UTC (0800-1200 local time) were played back as background traffic, meaning that these aircraft in the simulation flew exactly as the corresponding real traffic on the date.

A representative aircraft, the Cessna 208B Grand Caravan (C208), was simulated as the UA. This aircraft is the most used in regional air cargo in the United States [22]. In each simulation, eleven UA, spaced in 10-minute increments, were flown from the origin airport with no conflict resolution active. The nominal routes provide information about interaction with different background traffic in a "do nothing" scenario.

### D. Scenario Evaluation Metrics

The impact on safety is measured using the *number of Losses of Separation (nLOS)* metric. nLOS is defined as the number of pairs of aircraft coming within 3 nautical miles (nmi) horizontally and 1000 feet (ft) vertically inside the terminal airspace. Outside the terminal airspace, the horizontal separation requirement increases to 5 nmi. It is noted that nLOS here is a proxy for detected conflicts. A loss of separation, as defined in this work, therefore signifies the potential workload needed to resolve the conflict. Ensuring safe operation is expected to affect the system's performance. Current LC2L procedures can sometimes result in significantly longer, inefficient routes. Therefore, the *Distance Travelled* along a trajectory by the UA under different route alternatives is measured and compared.

### E. Study Assumptions

The following assumptions are made:

- C208 is assumed to be an analog for all future UA aircraft. Other aircraft models can be tested in the future in NAS Digital Twin
- Each simulated UA had a cruise speed of 160 knots and a speed of 150 knots after the entry fix for arrival is

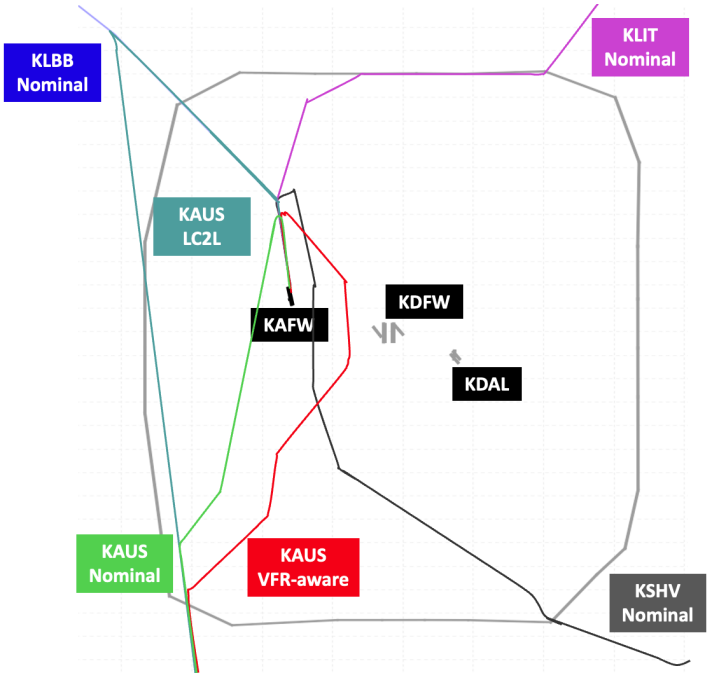


**Fig. 4 D10 TRACON (grey polygon) and airports of interest (black labels) along with the different nominal routes used in this study. LC2L and VFR traffic-aware route alternatives for the UA flights from KAUS are also shown. D10 is approximately 70 nmi x 70 nmi in size.**

reached.

– To investigate a "worst case scenario" wherein the arrival airspace is busiest, simulation times were adjusted so that the first UA in each simulation enters D10 during the normally busy morning rush hour.

For each of the four entries, five route alternatives were evaluated for a total of 20 test scenario simulations. Within each simulation, metrics are evaluated across 11 UA flights. The results compare the metrics for the five route alternatives for each direction of entry.

## III. Results

Fig. 5 shows the predicted VFR traffic interaction risk within 50 miles of KAFW during the morning rush hour. It is used to create an example VFR traffic risk-aware route (also shown on the map) for a UA coming from KAUS and entering D10 form the southwest corner post at SLUGG. Similarly, IFR traffic risk-aware and all traffic risk-aware routes were generated for each of the four corner posts as described under section II.C.

Results are presented for scenarios originating from four different airports: KAUS (Southwest entry), KLBB (Northwest entry), KLIT (Northeast entry), and KSHV (Southeast entry). Five scenarios were evaluated in NAS Digitial Twin for each airport (entry direction) - 'Nominal' area navigation (RNAV) approach (how a UA would fly in nominal conditions), an 'LC2L' RNAV approach (how a UA would fly during LC2L following DO-400 direct-to-IAP procedure), 'IFR-aware' (minimizing cost of IFR traffic interaction risk), 'VFR-aware' (minimizing cost of VFR traffic interaction risk), and 'IFR+VFR-aware' (minimizing cost of all traffic interaction risk in the airspace).

Fig. 6 shows the distribution of the average nLOS across the 20 scenarios (5 scenarios per airport). Overall, traffic interaction risk-aware routing reduced nLOS compared to the Nominal and LC2L baseline scenarios. VFR-aware trajectories showed a lower nLOS than IFR-aware ones in general, except for the case of KLIT. The airspace between the northeast entry and KAFW tended to have less VFR traffic, and so the VFR-aware routes were more direct from this direction than the IFR-aware routes. However, significant legacy background IFR traffic passes this region, and hence, a higher nLOS was observed. Accounting for all traffic also showed an overall reduction in nLOS. However, it performed slightly worse than either of the other traffic-type-specific interaction risk-aware routes.

It was also observed that flights from the west (KAUS, KLBB) had less nLOS than those from the east (KLIT, KSHV). The difference could be explained by the longer distance that the traffic from the east must travel through the busy TRACON airspace, increasing exposure and conflict risk compared to the shorter, more direct paths from the west.

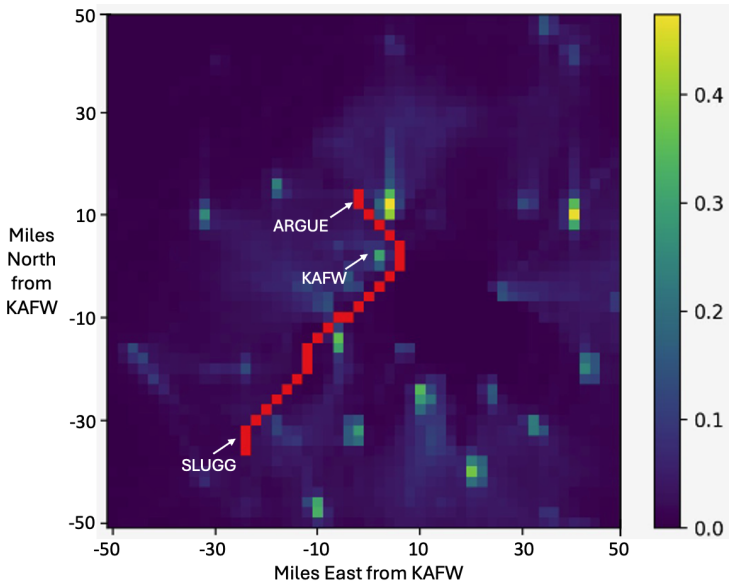


**Fig. 5 VFR interaction risk map and the trajectory to minimize interaction risk. D10 Tracon entry fix SLUGG, Intermediate Fix ARGUE on the final approach to runway 16L, and the KAFW airport locations are shown for reference.**

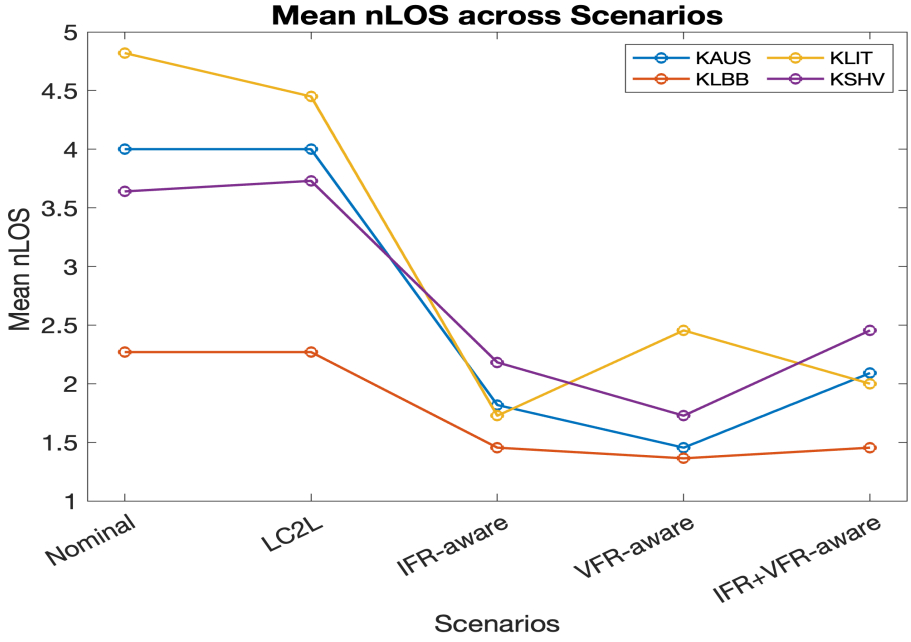


**Fig. 6 Distribution of average number of losses of separations encountered for all scenarios.**

Fig. 7 shows the distribution of the average distance traveled by the UA across the 20 scenarios. IFR-aware trajectories outperformed baseline trajectories, with particularly notable reductions for arrivals from KSHV and KLIT. VFR-aware routes in general were slightly longer than IFR-aware ones but comparable or better than the baseline trajectories. Since the VFR traffic tends to be more distributed and less structured than IFR traffic, avoiding it is expected to create longer route alternatives.

Contrary to the safety case, eastern entries (KLIT, KSHV) demonstrated notable distance reductions as compared to the western entries (KAUS, KLBB). This is explained by the same reasoning as before. The eastern routes, being

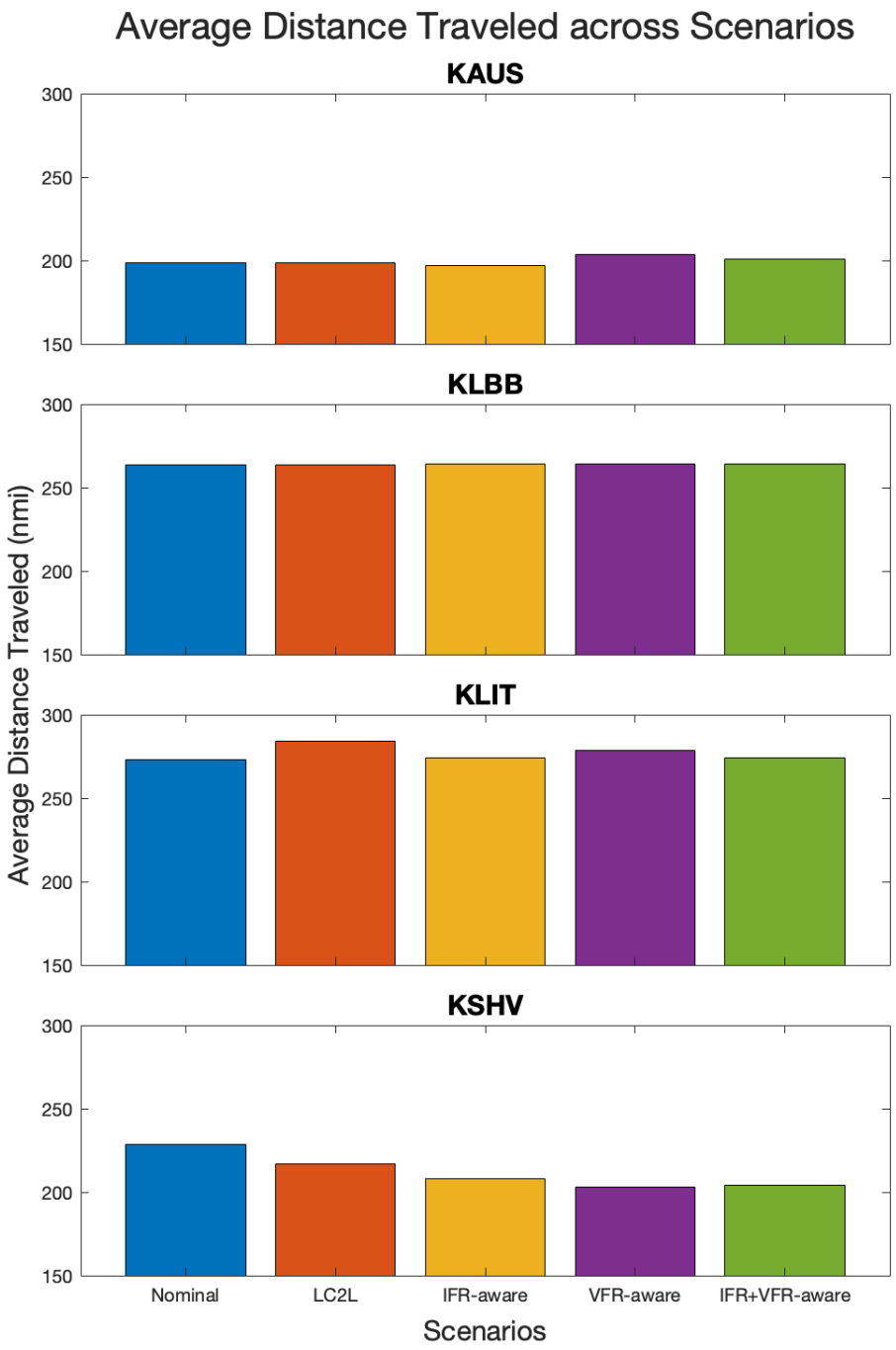


**Fig. 7 Distribution of average distance traveled for all scenarios.**

longer, also provide more opportunity for direct routing and distance reduction through the airspace. However, it is noted that the proposed approach does not currently restrict any areas as no-fly zones (e.g., class B airspace), and UA can fly diagonally through the TRACON directly over Dallas Fort Worth for example. In real-world integration of UAS, such access may be restricted to some extent, although the UAS are expected to operate under IFR [2].

## IV. Conclusions

This work proposed and evaluated a traffic interaction risk-aware routing of uncrewed aircraft during a contingency. Loss of command and control link was the contingency modeled. Amidst contingency, uncrewed aircraft were routed based on traffic interaction risk derived from the last known traffic predictions in the airspace en route to a destination.

For the chosen study region of KAFW terminal airspace, these risk-aware routes were compared with baseline routes using fast-time simulations. Impacts on safety and operational efficiency were measured. Five scenarios (two baseline and three traffic interaction risk-aware) for each direction of entry into the TRACON were evaluated.

Overall, the results showed a reduction in potential conflicts while also reducing the distance traveled in most test cases. VFR-aware routing performed marginally better on safety than IFR-aware routing. However, IFR-aware routes reduced the distance traveled more than VFR-aware routes while keeping the potential for conflicts comparable. The benefits were similar if both VFR and IFR traffic were jointly considered. At the same time, the method allowed for routing around both IFR and VFR traffic, which in itself is a novel approach.

The work suggests that dynamic, context-aware contingency routing informed by predictive airspace metrics could inform conflict avoidance and overall safety of UA integration. Such routing for LC2L contingencies offers potential benefits for safety and efficiency over current standard procedures. The traffic interaction risk-aware routing can be further evaluated with other criteria for safety and performance. Other such metrics could also be evaluated using this framework. An accompanying work by the authors characterizes another complexity metric informed by communication task load [10] and compares its performance alongside traffic interaction risk-aware routing. While they were compared in that study for contingency UA operations, both metrics may provide contributions to mitigating conflict risk even in non-contingency situations.

It was also observed that specific safety and efficiency impacts depend on the airspace context and baseline route attributes, such as longer TRACON transits. Limitations of this study, therefore, include metric maps not yet fully incorporating all real-world operational constraints (e.g., strict airspace class avoidance, weather, etc.). Future work should prioritize refining metric maps with these constraints and exploring more techniques for multi-utility optimization, partly explored in the accompanying work by the authors.

## Acknowledgments

This work was conducted at the NASA Ames Research Center and funded by NASA's Air Traffic Management eXploration (ATM-X) Project and Pathfinding for Airspace with Autonomous Vehicles (PAAV) sub-project. The authors sincerely thank David Thipphavong, Richard Coppenbarger, and Aastha Acharya from NASA Ames Research Center, and Anahita Jain from the University of Texas, Austin, for their support with the research. Our gratitude also extends to SME's Scott Howe and Wayne Bridges, both formerly from NASA, for their expertise on operational procedures and metric interpretation. The teams managing the NASA Sherlock Data Warehouse and the NAS Digital Twin environment, both at NASA Ames Research Center, provided essential support. The authors specifically thank Todd Lauderdale, Robert Windhorst, James Phillips, Christian Plaunt, and Chok Fung Lai.

## References

[1] Andrews, J., Lara, M., Yon, R., Del Rosario, R., Block, J., Davis, T., Hasan, S., Weingart, D., Frankel, C., Spitz, B., et al., "LMI automated air cargo operations market research and forecast," *NASA Contractor Report - 20210015228*, 2021.

[2] Hayashi, M., Idris, H., Sakakeeny, J., and Jack, D., "PAAV Concept Document," 2022.

[3] RTCA, "DO-377B," 2023.

[4] Organization, I. C. A., "Progress of Lost C2 Link and Detect and Avoid (DAA) Procedures (RPASP/16-WP/15)," 2023.

[5] RTCA, "DO-400: Standardized Lost C2 Link Procedures for Uncrewed Aircraft Systems," 2023.

[6] Sakakeeny, J., Thipphavong, D., Lauderdale, T., and Idris, H., "Initial Assessment of Lost Command and Control Link Procedures," *43rd Digital Avionics Systems Conference (DASC)*, 2024.

[7] Bulusu, V., Idris, H., and Acharya, A., "Analysis and prediction of VFR vs IFR traffic behavior to support uncrewed aircraft flight operations at regional airports," *AIAA AVIATION FORUM AND ASCEND 2024*, 2024, p. 4551.

[8] Bulusu, V., Idris, H., and Chatterji, G., "Analysis of VFR traffic uncertainty and its impact on uncrewed aircraft operational capacity at regional airports," *AIAA Aviation 2023 Forum*, 2023, p. 3553.

[9] Acharya, A., Bulusu, V., and Idris, H., "VFR Trajectory Forecasting using Deep Generative Model for Autonomous Airspace Operations," *43rd Digital Avionics Systems Conference (DASC)*, 2024.

[10] Dimitrova, N., Bulusu, V., Sakakeeny, J., and Idris, H., "Minimizing communication task load and traffic interaction risk in uncrewed aircraft contingency management," *AIAA AVIATION FORUM AND ASCEND 2025*, 2025.

[11] Lauderdale, T. A., Windhorst, R. D., Coppenbarger, R., Thipphavong, D. P., and Erzberger, H., "The National Airspace System (NAS) Digital Twin Simulation Environment," *AIAA AVIATION FORUM AND ASCEND 2024*, 2024, p. 4011.

[12] Palopo, K., Chatterji, G. B., Guminsky, M. D., and Glaab, P. C., "Shadow mode assessment using realistic technologies for the national airspace system (SMART NAS) test bed development," *AIAA Modeling and Simulation Technologies Conference*, 2015, p. 2794.

[13] Robinson III, J. E., Lee, A., and Lai, C. F., "Development of a high-fidelity simulation environment for Shadow-Mode Assessments of Air Traffic Concepts," *Aeronautical Society Modeling and Simulation in Air Traffic Management Conference*, 2017.

[14] Emmerich, M. T., and Deutz, A. H., "A tutorial on multiobjective optimization: fundamentals and evolutionary methods," *Natural Computing*, Vol. 17, 2018, pp. 585–609.

[15] Folland, G. B., *Real Analysis: Modern Techniques and Their Applications*, 2nd ed., John Wiley Sons, 1999.

[16] Wikipedia contributors, "Pareto front - Wikipedia, The Free Encyclopedia," , 2024. URL `https://en.wikipedia.org/wiki/Pareto_front`.

[17] Zhang, J., et al., "Random Hypervolume Scalarizations for Provable Multi-Objective Black Box Optimization," *Proceedings of Machine Learning Research*, Vol. 119, 2020, pp. 11088–11097. URL `http://proceedings.mlr.press/v119/zhang20i/zhang20i.pdf`.

[18] Golovin, D., and Zhang, Q. R., "Random Hypervolume Scalarizations for Provable Multi-Objective Black Box Optimization," *ACM Digital Library*, 2020. URL `https://dl.acm.org/doi/pdf/10.5555/3524938.3525967`.

[19] Zhang, Q. R., "Optimal Scalarizations for Sublinear Hypervolume Regret," *arXiv*, 2024. URL `https://arxiv.org/pdf/2307.03288.pdf`.

[20] Morris, B., and Powell, A., "Sufficient Conditions for the Lipschitz Continuity of QP-based Multiobjective Control," *CDC Proceedings*, 2013. URL `http://ames.caltech.edu/morris_powell_ames_2013cdc.pdf`.

[21] Gebken, B., and Peitz, S., "An efficient descent method for locally Lipschitz multiobjective optimization problems," *arXiv*, 2020. URL `https://arxiv.org/abs/2004.11578`.

[22] Sakakeeny, J., Sievers, T. F., and Idris, H., "Potential of United States and European regional air cargo operations for uncrewed aircraft systems," *15th USA/Europe Air Traffic Management Research and Development Seminar (ATM2023)*, 2023.

[23] "FAA Sectional Chart for Dallas-Fort Worth Area," `https://www.faa.gov/air_traffic/flight_info/aeronav/productcatalog/VFRCharts/Sectional/`, 2023. Images produced by the U.S. Government and in the public domain.

# A. Traffic Scenarios

**Table 1 Nominal UAS RNAV (GPS) Routes to KAFW.**

| Origin Airport | Flight Plan | Corner post |
|---|---|---|
| KLBB | KLBB .. TURKI .. CDS .. SPS .. UKW .. MOTZA .. RAVYA .. ARGUE .. WIGZU .. KAFW | NW |
| KAUS | KAUS .. BIEST .. HRLIP .. FOSSL .. SLUGG .. LIKES .. RAVYA .. ARGUE .. WIGZU .. KAFW | SW |
| KLIT | KLIT .. PONYY .. MELTE .. CAINE .. SASIE .. BLECO .. TRUUK .. RAVYA .. ARGUE .. WIGZU .. KAFW | NE |
| KSHV | KSHV .. VDUBB .. DODJE .. REEKO .. SWVAY .. SCOPS .. LIKES .. RAVYA .. ARGUE .. WIGZU .. KAFW | SE |

**Table 2 DO-400 UAS RNAV (GPS) LC2L Contingency Routes to KAFW.**

| Origin Airport | Flight Plan | Corner post |
|---|---|---|
| KLBB | KLBB .. TURKI .. CDS .. SPS .. UKW .. MOTZA .. RAVYA .. ARGUE .. WIGZU .. KAFW | NW |
| KAUS | KAUS .. BIEST .. HRLIP .. FOSSL .. SLUGG .. LIKES .. RAVYA .. ARGUE .. WIGZU .. KAFW | SW |
| KLIT | KLIT .. PONYY .. MELTE .. CAINE .. SASIE .. BLECO .. TRUUK .. RAVYA .. ARGUE .. WIGZU .. KAFW | NE |
| KSHV | KSHV .. VDUBB .. DODJE .. REEKO .. SWVAY .. SCOPS .. RAVYA .. ARGUE .. WIGZU .. KAFW | SE |

**Table 3 Metric-aware UAS LC2L Contingency Routes to KAFW.**

| Origin Airport | Flight Plan | Corner post |
|---|---|---|
| KLBB | KLBB .. TURKI .. CDS .. SPS .. UKW .. MOTZA .. [metric-informed] .. ARGUE .. WIGZU .. KAFW | NW |
| KAUS | KAUS .. BIEST .. HRLIP .. FOSSL .. SLUGG .. [metric-informed] .. ARGUE .. WIGZU .. KAFW | SW |
| KLIT | KLIT .. PONYY .. MELTE .. CAINE .. SASIE .. [metric-informed] .. ARGUE .. WIGZU .. KAFW | NE |
| KSHV | KSHV .. VDUBB .. DODJE .. [metric-informed] .. ARGUE .. WIGZU .. KAFW | SE |